EXPERIMENTAL STUDY OF CHARGING AND MOBILISATION OF DUST GRAINS ON BEAM SCREEN SURFACES

P. Ziegler*,[1,2], M. Himmerlich[2], P. Krkotić[2], M. Horanyi[4], X. Wang[4], C. Wiesner[2], D. Wollmann[2], R. Schmidt[3], H. Podlech[1,5]
[1]Goethe-Universität Frankfurt am Main, Frankfurt am Main, Germany
[2]CERN, Geneva, Switzerland
[4]LASP, University of Colorado Boulder, Boulder, CO, USA
[3]Technische Universität Darmstadt, Darmstadt, Germany
[5]Helmholtz Research Academy Hesse for FAIR (HFHF), GSI Helmholtzzentrum für Schwerionenforschung, Campus Frankfurt, Germany

Abstract

Beam losses caused by interactions between the circulating beam and dust grains have been observed at many particle accelerators, leading to premature beam dumps, quenches of superconducting magnets, and vacuum pressure bursts. At some facilities, these events have a significant impact on the overall accelerator performance. The mechanisms by which dust grains detach from vacuum-chamber surfaces and enter the beam are not yet fully understood; one possible process is charge build-up on the grain followed by lofting due to the beam potential. We present an experimental study of the charging and mobilisation of silica dust on accelerator-relevant surfaces: Cu, co-laminated Cu, laser-treated Cu, NEG-coated substrates and samples treated with VacSeal, a silicone-based resin widely used to seal vacuum leaks. The observations provide input for dust-dynamics simulations and studies of beam losses.

INTRODUCTION

Dust particles mobilised from vacuum-chamber surfaces have caused beam losses at numerous particle accelerators, including the LHC [1–3] and SuperKEKB [4–7]. Such events can trigger premature beam dumps, quench superconducting magnets, and cause vacuum pressure bursts, significantly impacting accelerator performance.

The mechanisms leading to dust detachment and subsequent beam interaction remain poorly understood. One proposed process involves negative charging of dust grains due to interaction with synchrotron radiation or electron clouds and subsequent electrostatic lofting. This process was demonstrated in Refs. [8–10] using UV light to mimic the effects of synchrotron radiation.

This study presents experimental results on dust charging and mobilisation from accelerator-relevant surfaces. Dust is deposited onto grounded substrates in a vacuum chamber and exposed to a homogeneous electric field. Grains were charged using UV light and their motion was recorded with a high-speed camera. The trajectories are reconstructed to extract charge-to-mass ratios and launch velocities. Different behaviours were observed on conductive and insulating surfaces. In addition, the insulating VacSeal layer exhibited discharge events. VacSeal is of interest because it was found inside the SuperKEKB beam pipe and is believed to be correlated with sudden beam losses [6].

* philipp.ziegler@cern.ch

EXPERIMENTAL SETUP

The experiments were performed in a cylindrical vacuum chamber 30 cm high and 30 cm in diameter at a pressure of $\sim 1.2\times10^{-5}$ mbar (see Fig. 1). The electric field was oriented toward the substrate to mimic positively charged beams, and reversed (toward the mesh) to represent negatively charged beams.

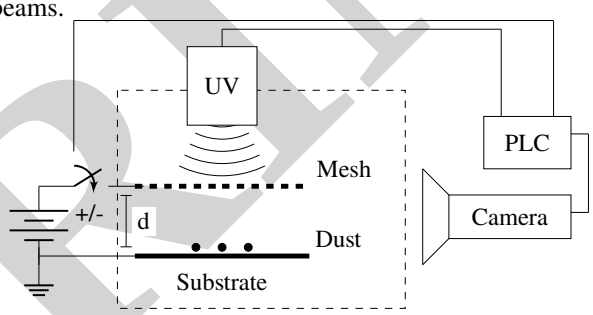

Figure 1: Schematics of the experimental setup. Dust grains are deposited on the grounded substrate. A Programmable Logic Controller (PLC) allows control of the high voltage (HV), the UV source [11] and of the triggering of the high-speed camera.

A conductive mesh with radius R_{mesh} = 5 cm was placed at a distance d = 1.7 cm above an electrically grounded sample (substrate). A bias voltage $\Phi = \pm 2$ kV was applied.

All substrates used oxygen-free (OFE) copper [12] as base material. The surface properties and the dust-lofting results are summarised in Table 1. They include bare Cu-, co-laminated Cu (75 µm) on stainless steel (representative of the LHC beam screen [13]) and laser-treated Cu in cleaned (LESS 1) and non-cleaned (LESS 2) states, both with groove depths of [15 – 25] µm [14]. Additionally, 70 nm Ti, 250 nm non-evaporable getter (NEG), and 50 nm amorphous carbon (a-C.) [15] coating as well as an insulating 71 µm-thick Kapton tape [16] and a thin film of VacSeal (VS), a silicone-resin-based vacuum sealant [17], were used.

For LESS 1 and LESS 2, the values in Table 1 are effective conductivities derived from measured surface resistances. They describe the laser-treated surface rather than

Table 1: Overview of Samples and Experimental Results

Sample	σ (MS/m)	Y	med(y_{max}) (mm)	med(Δt_{rise}) (ms)	med$(q/m)_{\uparrow}$ (mC/kg)	med$(q/m)_{\downarrow}$ (mC/kg)	Num. Traj.
Cu	58–59.6 [18]	10^{-4} [19] $^{+}$ / 0.03 [20]*	5.3	10.8	-0.84	1.55	26
Co-lam. Cu	58–59.6 [18]	0.07 [20]*	5.5	9.1	-1.34	1.82	381
LESS 1	37–47 [14]	0.05 [20]*	4.6	9.4	-1.05	1.40	1152
LESS 2	53.5 [14]	-	6.1	10.3	-0.77	1.09	2836
Cu–Ti	2.4 [15]	0.11–0.15 [21]‡	5.8	12.7	-0.73	0.89	31
Cu–NEG	0.05–1 [15, 22]	0.04 [23]†	5.9	12.4	-0.90	1.11	670
a-C.	0.001–0.01 [15, 24]	0.01 [23]†	6.2	8.6	-1.26	1.38	18
Kapton	≈ 0	~ 10^{-4} [25]$^{+}$	5.5	4.5	-1.01	2.36	45
VS 1	≈ 0	-	6.7	12.4	-0.88	1.14	197
VS 2	≈ 0	-	-	1.5	-17.5	-	5

Note: The table lists the reported conductivity σ, quantum efficiency Y, median lofting height y_{max}, median dust rise time Δt_{rise}, median charge-to-mass ratio q/m during upward (↑) and downward (↓) motion, and the number of analysed trajectories after filtering. Estimates for Y are marked as follows: $^{+}$ 172 nm, * white light, † LHC injection synchrotron radiation, and ‡ KEKB positron-beam synchrotron radiation.

the DC bulk conductivity of the OFE copper substrate. Here, 'cleaned' denotes a passivated surface without nanoparticulates, while 'non-cleaned' denotes a nanoparticulate layer mainly composed of Cu and CuO. For Cu–Ti and Cu–NEG, the listed conductivities correspond to the Ti and NEG coatings, respectively, not to the full multilayer system.

Monolayers of pure silica dust grains with diameters below 50 µm and density $\rho = 2.196\,\mathrm{g/cm^3}$ [26] were dispersed on the substrate. A 172 nm UV source with an intensity of 35 mW/cm^2 [11] corresponding to a flux of $\Phi_{ph} = 3.0\times10^{20}$ photons/(m^2 s) was placed above the mesh and illuminated the substrate.

A programmable logic controller (PLC) [27] synchronized the high voltage, UV illumination, and triggering of a high-speed camera operating at up to 5300 frames per second. To ensure steady conditions, the UV illumination and camera trigger were delayed by 5 s after the high voltage was switched on. The local electric potential above the substrate was measured with an emissive probe [28], limited to mesh voltages up to 100 V. Currents from both the emissive probe and power supply were recorded with a 2 ms sampling time.

Dust detection and trajectory reconstruction were performed in Fiji [29] using the TrackMate plugin [30, 31]. Trajectories were filtered to include only the ones spanning at least 20 frames (≈ 6 ms with 3300 frames-per-second) and reaching a vertical distance greater than 1 mm, and smoothed using a constant--acceleration Kalman filter [32].

RESULTS

Dust charge

On all substrates, the dust was observed to move. When applying $\Phi = -2$ kV to the mesh and illuminating the sample with UV light, some dust grains were lofted and then accelerated by the electrical field directly towards the mesh. In this case, dust needs to be positively charged. With +2 kV applied to the mesh and active UV illumination, dust grains were lofted but returned to the surface, following parabolic trajectories as observed in [9]. The following analysis of dust trajectories is focussed on measurements with $\Phi = +2$ kV.

Detailed analysis showed that the acceleration of the dust grains is not constant. Dust grains follow a parabolic trajectory with a median rise time (med(Δt_{rise})), i. e. time from substrate to the highest point, of approximately 10 ms and a fall time, i. e. time from the highest point down to substrate, of approximately 5 ms. Here, the median of all analysed dust trajectories per video is taken. The number of trajectories ranges between 18 – 2836 (see Table 1).

The motion can be split into three phases. Phase 1 describes the initial negative charging of the dust grain. This is consistent with the Patched Charge Model (PCM) [33, 34]. In the PCM, photoelectrons emitted from the substrate are absorbed within micro-cavities at the grain–surface contact, resulting in negative net grain charge.

Since the exact size of the dust grain is not well known, the charge-to-mass ratios are analysed, given by:

$$ma_y = -qE_y - mg \quad \Leftrightarrow \quad \frac{q}{m} = -\frac{\mathrm{d}}{\Phi}\,(a_y + g), \qquad (1)$$

where g is the gravitational acceleration, $E_y = \Phi/\mathrm{d}$ the vertical electric field, and a_y denotes the vertical acceleration obtained from the videos. From the reconstructed trajectories obtained by high-speed imaging, initial q/m values of about $-0.15\,\mathrm{mC/kg}$ are derived for individual grains and are similar across all substrates.

In phase 2, the grains are lofted and accelerated towards the +2 kV-biased mesh after overcoming adhesion, gravity, and the image force, i. e. the force between the dust grain and its induced mirror charge. The rising grain continues to interact with photoelectrons emitted from the substrate, which are accelerated by the electric field and therefore impact the grain with increasing energy. The median of the maximum med$(q/m)_{\uparrow}$ values per trajectory is given in Table 1.

Below a height of approximately 100 µm, the impacting photoelectrons have an energy of less than 15 eV, for which a secondary electron yield of the dust grain of $\delta \sim 0.7$ is assumed [35]. The negative charging current of the dust due to absorbed photoelectrons is thus given by

$$I_{se} = (\delta - 1) I_{pe,\,meas.} \frac{A_{dust}}{A_{mesh}} \in [-9,\,-1]\,\mathrm{pA}, \qquad (2)$$

where $A_{\mathrm{mesh}} = \pi R_{\mathrm{mesh}}^2$ is the surface area of the mesh and $A_{\mathrm{dust}} = \pi r_{\mathrm{dust}}^2$ the cross-sectional area of the dust grain with radius $r_{\mathrm{dust}} \in [10-25]\,\mu\mathrm{m}$. With the measured photocurrent $I_{\mathrm{pe,\,meas.}} = 125\,\mu\mathrm{A}$ between substrate and mesh, the derived median negative q/m value of about $-0.7\,\mathrm{mC/kg}$ for Cu would be reached after approximately $[4-10]$ ms.

In phase 3, the photoelectrons have sufficiently high energies to ionise the dust through secondary electron emission. From [35–39], the secondary electron yield $\delta \in [1, 3]$ at an impact energy of $[0.015-2.3]$ keV, causing net electron loss and thus ionisation of the dust grain. This results in a theoretical ionisation time $\Delta t \in [4-11]$ ms for the observed $\Delta q/m = 2.3\,\mathrm{mC/kg}$ within the observation time window and explains the parabolic trajectories.

In general, similar dust mobility was observed for all studied conductive substrates, except for a-C. coating, which has a lower photoelectron yield and showed a much lower dust mobility compared to the other substrates.

Conductive and insulating surfaces

We observed the following for dust on conductive and insulating substrates: On insulating Kapton, lofting stopped after about 600 ms, whereas on the conductive LHC beam screen substrate it continued for about 3 s. This is consistent with positive charge accumulation on the insulating substrate. As the surface potential rises towards the mesh bias, the electric field between substrate and mesh decreases and eventually becomes too weak to lift further dust grains.

To verify this, the local potential a few mm above the grounded co-laminated Cu (Conductor) and the Kapton (Insulator) substrate was measured with an emissive probe during UV irradiation with a mesh voltage of 100 V. As shown in Fig. 2, the potential above the conductive surface remained nearly constant, while above the insulating surface it increased from about 20 V to 60 V within 600 ms, decreasing the effective mesh to substrate voltage difference.

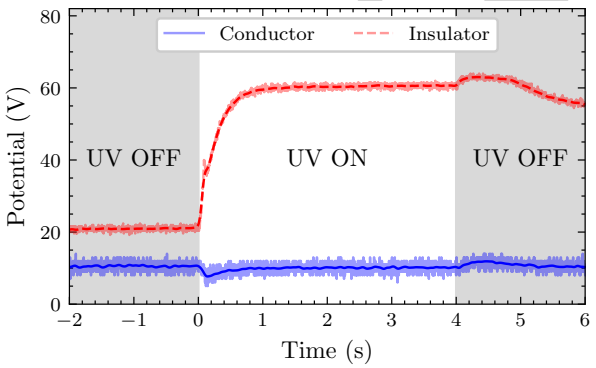

Figure 2: Variation of the local potential above a conductive (blue) and insulating (red) surface during UV irradiation.

Dust on VacSeal

It was hypothesised that VS could trigger sudden beam loss events at SuperKEKB [6, 40]. In the laboratory experiment, liquid VS was painted onto co-laminated Cu and left to dry for several days (VS 1 in Table 1). A second sample was irradiated with electrons of energy ≈ 135 eV for several days. In both cases, the VS turned white, less transparent, and developed a sticky surface, while electron bombardment caused no additional surface changes.

The dust motion on VS 1 was similar to that on the other substrates. However, lofting required only $\approx 41\,\mathrm{kV/m}$, about a factor of two lower than elsewhere. This is explained by a reduced image force due to the finite VS thickness. After few min of UV irradiation, another mechanism was observed: fast, bright glowing spots appeared for less than 0.2 ms on the surface. These spots were also detected in regions without silica grains. Measurements of VS under prolonged UV illumination are labelled VS 2 in Table 1.

In the consecutive frames after the bright spot had appeared, several small, very fast objects moved away in all directions with a speed of $v_0 \approx [4-8]\,\mathrm{m/s}$, a factor 4 – 6 faster than regular dust corresponding to q/m of $\approx 17.5\,\mathrm{mC/kg}$.

Applying the algorithm from [41] to nominal beam parameters shows that typical dust sizes and pre-charges do not reach the beam centre. In contrast, the high v_0 observed for VS 2 allows full beam penetration, since ionisation alone cannot stop the fragments. This provides a plausible transport mechanism for dust reaching the beam centre, as assumed for the study of sudden beam losses in [40].

CONCLUSION

Laboratory experiments were performed to obtain a comprehensive picture of dust charging and release mechanisms from different accelerator-relevant surfaces. For set-ups mimicking positive beams it was found that dust grains acquire an inhomogeneous negative charge before overcoming gravitational, adhesive, and image forces and being released from the surface. The charge does not remain constant, but changes due to the continued impact of photoelectrons with increasing energy leading to secondary electron emission. Of all conductive substrates, Cu with a-C. coating showed the lowest dust mobility. This is consistent with a lower charging rate through PCM, as it has a lower photoelectron yield. Distinct behaviour was observed with a thin VS layer on top of a conductive substrate. Discharges at the VS surface ejected fast particulates. Unlike dust grains with typical initial charges and velocities, these ejected fragments would be fast enough to reach the centre of a high-intensity particle beam and could be a mechanism to explain the sudden beam losses observed at SuperKEKB.

ACKNOWLEDGEMENTS

This work is supported by the Wolfgang Gentner Programme of the German Federal Ministry of Education and Research (grant no. 13E18CHA), CERN's TE-MPE group, and NASA SSERVI's Institute for Modeling Plasma, Atmospheres, and Cosmic Dust (IMPACT, grant no. 80NSSC19M0217). We thank Leonhard Guenther for support with the microscopy measurements.

REFERENCES

[1] A. Lechner and F. Cerutti, "FLUKA simulations of UFO–induced losses in the LHC arc", in *Meeting of the LHC UFO study group*, Apr. 2012.

[2] A. Lechner *et al.*, "Beam Loss Measurements for Recurring Fast Loss Events During 2017 LHC Operation Possibly Caused by Macropartaicles", in *Proc. IPAC'18*, Vancouver, Canada, Apr.-May 2018, pp. 780–783. doi:10.18429/JACoW-IPAC2018-TUPAF040

[3] A. Lechner *et al.*, "Dust-induced beam losses in the cryogenic arcs of the CERN Large Hadron Collider", *Phys. Rev. Accel. Beams*, vol. 25, no. 4, p. 041001, Apr. 2022. doi:10.1103/PhysRevAccelBeams.25.041001

[4] S. Terui *et al.*, "Report on Collimator Damaged Event in SuperKEKB", in *Proc. IPAC'21*, Campinas, Brazil, May 2021, pp. 3541–3544. doi:10.18429/JACoW-IPAC2021-WEPAB359

[5] H. Ikeda *et al.*, "Observation of sudden beam loss in SuperKEKB", in *Proc. IPAC'23*, Venice, Italy, pp. 716–719, Sep. 2023. doi:10.18429/JACoW-IPAC2023-MOPL072

[6] H. Ikeda *et al.*, "Observations and efforts to reduce sudden beam loss at SuperKEKB", in *Proc. IPAC'25*, Taipei, Taiwan, pp. 57–60, Jun. 2025. doi:10.18429/JACoW-IPAC25-MOCD3

[7] R. Nomaru, G. Mitsuka, and L. Ruckman, "Measurement of Sudden Beam Loss Events Using Bunch-by-Bunch BPMs at SuperKEKB", *J. Instrum.*, vol. 21, no. 03, T03008, Mar. 2026. doi:10.1088/1748-0221/21/03/T03008

[8] A. Elliott *et al.*, "Electrostatic dust lofting: a possible cause for beam losses at CERN's LHC", in *Proc. IPAC'23*, Venice, Italy, pp. 177–180, May 2023. doi:10.18429/JACoW-IPAC2023-MOPA065

[9] K. Taylor *et al.*, "Photoelectric charging and lofting of dust particles on a conducting surface with external electric fields", *Phys. Plasma*, vol. 31, no. 7, p. 073703, 2024. doi:10.1063/5.0210675

[10] K. Taylor, X. Wang, M. Horányi, R. Schmidt, C. Wiesner, and D. Wollmann, "Charging and lofting of dust particles on surfaces exposed to a pulsed electron beam", *Phys. Plasma*, vol. 32, no. 11, p. 113702, Nov. 2025. doi:10.1063/5.0291509

[11] Xeradex GmbH, "Technical information: xeradex l40/175/sb-sx48/kf50hv", https://pim.radiumserver.de/bme/t/i/ti2_xeradex_34317388.pdf,

[12] European Organization for Nuclear Research (CERN), "Technical Specification No. 2001 – Ed. 9: Oxygen-Free Electronic Copper Bars/Blanks/Ingots (Cu-OFE)", CERN, Rep. 2001, Jun. 2025. https://edms.cern.ch/ui/file/790779/7/Spec_2001_Ed._9_Cu-OFE_Forged_EDMS-790779.pdf

[13] P. Cruikshank *et al.*, "Mechanical Design Aspects of The LHC Beam screen", in *Proc. PAC'97*, Vancouver, Canada, pp. 3586–3588, May 1997. doi:10.1109/PAC.1997.753282

[14] P. Krkotić *et al.*, "Influence of nanoparticulates and microgrooves on the secondary electron yield and electrical resistance of laser-treated copper surfaces", *Phy. Rev. Accel. Beams*, vol. 27, no. 11, p. 113101, 2024. doi:10.1103/PhysRevAccelBeams.27.113101

[15] K. Brunner *et al.*, "Dielectric resonator to measure surface resistance of accelerator components at room temperature and 77 K", *Phy. Rev. Accel. Beams*, vol. 26, no. 8, p. 083101, 2023. doi:10.1103/PhysRevAccelBeams.26.083101

[16] Bron Aerotech, LLC., "BA 8886 Kapton® Tape / Acrylic Adhesive", https://bronaerotech.com/products/ba-8886,

[17] Kurt J. Lesker Company, "Vacseal – High Vacuum Leak Sealant", https://www.lesker.com/newweb/fluids/sealants-leaksealant-kjlc/vacseal/,

[18] European Organization for Nuclear Research (CERN), "Technical Specification No. 2001 – Ed. 9: Oxygen-Free Electronic Copper Bars/Blanks/Ingots (Cu-OFE)", CERN, Rep. 2001, Jun. 2025. https://edms.cern.ch/ui/file/790779/7/Spec_2001_Ed._9_Cu-OFE_Forged_EDMS-790779.pdf

[19] P. Davis *et al.*, "Quantum efficiency measurements of a copper photocathode in an rf electron gun", in *Proc. International Conference on Particle Accelerators 1993*, Washington, DC, USA, pp. 2976–2978, 1993. doi:10.1109/PAC.1993.309524

[20] E. La Francesca *et al.*, "Reflectivity and photoelectron yield from copper in accelerators", *Phys. Rev. Accel. Beams*, vol. 23, no. 8, p. 083101, 2020. doi:10.1103/PhysRevAccelBeams.23.083101

[21] Y. Suetsugu, K. Kanazawa, K. Shibata, and H. Hisamatsu, "Continued study on photoelectron and secondary electron yields of tin and NEG (Ti-Zr-V) coatings at the KEKB positron ring", in *Proc. PAC'07*, Albuquerque, NM, USA, pp. 4054–4056, 2007. doi:10.1109/PAC.2007.4439958

[22] S. Lemettre *et al.*, "Thermal activation of co-evaporated ti, zr and v-based binary and ternary getter alloy thin films: characterization by electrical measurements during hydrogenation", *Vacuum*, vol. 239, p. 114354, 2025. doi:10.1016/j.vacuum.2025.114354

[23] E. Buratin, V. Baglin, B. Henrist, P. Chiggiato, and A. Fasoli, "Electron flux and pressure dynamic in the LHC vacuum pilot sector as a function of beam parameters and beam pipe properties", *Phys. Rev. Accel. Beams*, vol. 23, no. 11, p. 114802, Nov. 2020. doi:10.1103/PhysRevAccelBeams.23.114802

[24] A. Passarelli, A. Andreone, M. D. Stefano, C. Koral, MR. Masullo, and VG. Vaccaro, "Broadband Frequency Electromagnetic Characterisation of Coating Materials", in *Proc. IPAC'21*, Campinas, SP, Brazil, pp. 1076–1079, Aug. 2021. doi:10.18429/JACoW-IPAC2021-MOPAB346

[25] J. Wu *et al.*, "Effects of Energetic Electron and Proton Irradiation on Electron Emission Yield of Polyimide Induced by Electron and Photon", *TRANSACTIONS OF THE JAPAN SOCIETY FOR AERONAUTICAL AND SPACE SCIENCES, AEROSPACE TECHNOLOGY JAPAN*, vol. 12, pp. 13–19, Jul. 2014. doi:10.2322/tastj.12.Pr_13

[26] MSE Supplies LLC, "MSE PRO Silicon Dioxide (Amorphous SiO_2) 99.99% (4N) High Purity Powder", https://www.msesupplies.com/products/mse-pro-silicon-dioxide-amorphous-sio-sub-2-sub-99-99-4n-high-purity-powder,

[27] Siemens AG, "LOGO! – the compact controller with a cloud interface", https://www.siemens.com/global/en/products/automation/systems/industrial/plc/logo.html,

[28] J. P. Sheehan and N. Hershkowitz, "Emissive probes", *Plasma Sources Science and Technology*, vol. 20, no. 6, p. 063001, Nov. 2011. doi:10.1088/0963-0252/20/6/063001

[29] J. Schindelin *et al.*, "Fiji: an open–source platform for biological–image analysis", *Nature Methods*, vol. 9, no. 7, pp. 676–682, 2012. doi:10.1038/nmeth.2019

[30] J.-Y. Tinevez *et al.*, "Trackmate: an open and extensible platform for single–particle tracking", *Methods*, vol. 115, pp. 80–90, 2017. doi:10.1016/j.ymeth.2016.09.016

[31] D. Ershov *et al.*, "Trackmate 7: integrating state–of–the–art segmentation algorithms into tracking pipelines", *Nature Methods*, vol. 19, no. 7, pp. 829–832, 2022. doi:10.1038/s41592-022-01507-1

[32] R. E. Kalman, "A New Approach to Linear Filtering and Prediction Problems", *ASME. J. Basic Eng.*, vol. 82, no. 1, pp. 35–45, 1960. doi:10.1115/1.3662552

[33] X. Wang, J. Schwan, H.-W. Hsu, E. Grün, and M. Horányi, "Dust charging and transport on airless planetary bodies", *Geophysical Research Letters*, vol. 43, no. 12, pp. 6103–6110, 2016. doi:10.1002/2016GL069491

[34] J. H. Pagán Muñoz *et al.*, "Charging and mobilization of dust particles on a surface in plasma", *Phys. Rev. Lett.*, vol. 133, no. 11, p. 115301, Sep. 2024. doi:10.1103/PhysRevLett.133.115301

[35] T. Tondu, M. Belhaj, and S. Zurbach, "Total electron emission yield of electric propulsion materials", in *Proc. 32nd International Electric Propulsion Conference (IEPC 2011)*, Wiesbaden, Germany, Sep. 2011. https://electricrocket.org/IEPC/IEPC-2011-105.pdf

[36] Y. C. Yong, J. T. L. Thong, and J. C. H. Phang, "Determination of secondary electron yield from insulators due to a low–kV electron beam", *J. Appl. Phys.*, vol. 84, no. 8, pp. 4543–4548, Oct. 1998. doi:10.1063/1.368700

[37] J. Cazaux, "e-induced secondary electron emission yield of insulators and charging effects", *Nucl. Instrum. Methods Phys. Res. B*, vol. 244, no. 2, pp. 307–322, 2006. doi:10.1016/j.nimb.2005.10.006

[38] P. Guo, SF. Mao, YB. Zou, TF. Yang, H. Miao, and ZJ. Ding, "Monte Carlo simulation study on secondary electron yield of SiO2", *Results in Physics*, vol. 58, p. 107472, 2024. doi:10.1016/j.rinp.2024.107472

[39] V. J. Belanger and A. E. Eagles, "Secondary emission conductivity of high purity silica fabric", in *NASA Lewis Research Center: Proceedings of the Spacecraft Charging Technology Conference*, Feb. 1977. https://ntrs.nasa.gov/citations/19780002225

[40] K. Ohmi, H. Fukuma, and S. Terui, "Beam-dust interactions in an e^+e^- collider", *Phys. Rev. Accel. Beams*, vol. 29, no. 2, p. 021002, Feb. 2026. doi:10.1103/dwmr-qldc

[41] P. Ziegler *et al.*, "Modelling Dust Grain Ionisation and Dynamics in Flat Lepton Beams Using a Sliced Approach", presented at IPAC'26, Deauville, France, May 2026, paper MOP1034, this conference.